A Spiking Neuron Model of Head-Direction Cells for Robot Orientation

Thomas Degris[*]   **Loïc Lachèze**[*]   **Christian Boucheny**[**]   **Angelo Arleo**[**]

[*]AnimatLab - LIP6
8 rue du Capitaine Scott
75015 PARIS
thomas.degris@lip6.fr
loic.lacheze@lip6.fr

[**]LPPA - Collège de France - CNRS
11 place M. Berthelot
75005 PARIS
angelo.arleo@college-de-france.fr
christian.boucheny@college-de-france.fr

Abstract

This paper proposes a bio-mimetic model of head-direction (HD) cells implemented on a real robot. The model is based on spiking neurons to study the temporal aspects of state transitions of the HD cell activity following reorienting visual stimuli. The short transient latencies observed experimentally are reproduced by the model. We focus on the integration of angular velocity inertial signals provided by accelerometers. This integration is realized by a continuous attractor network modeling the interaction between the lateral mammillary nucleus (LMN) and the dorsal tegmental nucleus (DTN), two structures belonging to the HD cell anatomical circuit. Relevant parameters defining the connections between LMN and DTN are determined by a genetic algorithm.

1. Introduction

Self-orienting agents, that is navigating systems able to estimate their own orientation autonomously and on-line, might rely upon an internal direction representation. Extracellular recordings from freely-moving rats show the presence of head-direction (HD) cells, limbic neurons whose firing activity is correlated with the current direction of the head of the animal (Taube, 1998). A HD cell n has a unique preferred direction θ_n for which it discharges maximally. The directional coding of the HD cells is independent of the animal location, and provides, therefore, an allocentric directional representation.

The properties of the HD cell system resemble those of a compass, but the allocentric coding of HD cells does not depend on geomagnetic fields. Rather, the preferred directions are anchored to visual cues in the environment. For instance, rotating a dominant visual cue by an angle $\Delta\theta$ causes a shift $\Delta\theta$ of all the preferred directions of the HD cells (Taube, 1998, Zugaro et al., 2001). Besides the control of visual cues upon HD cells, experiments show that inertial self-motion signals (e.g. vestibular) strongly influence the dynam-

ics of the HD cell system. For instance, when the environmental light is turned off, the directional coding is maintained (Taube, 1998). In addition, when the head of the animal rotates, vestibular signals (coding for the head angular velocity ω) are integrated to update the HD representation over time.

HD cells have been observed in several regions centered on the brain limbic system, in particular the post-subiculum (PSC), the anterodorsal thalamic nucleus (ADN), and the lateral mammillary nucleus (LMN) (Taube, 1998). Inertial self-motion signals are likely to converge onto the HD system via the dorsal tegmental nucleus (DTN) (Bassett and Taube, 2001) which projects inhibitory connections directly to LMN. Visual inputs enter the HD system via the PSC which receives afferents from the visual cortex (Taube, 1998). Fig. 1 shows the anatomical interconnections between PSC, ADN, LMN and DTN.

Maintaining a sense of direction autonomously is crucial for both biological and artificial systems involved in navigation. For instance, path integration allows a navigating agent to infer its location and its heading relative to a departure point (Mittelstaedt and Mittelstaedt, 1980). This implies estimating the rotational as well as the translational components of motion continuously. In addition, lesions to the HD cell system disrupt the allocentric location representation of hippocampal place cells (Knierim et al., 1995), neurons whose firing activity is correlated with the location of the animal. Consequently, the sense of direction is necessary for establishing place cell representations.

This paper presents a neuro-mimetic model of the HD system and focuses on its robotic implementation. To reflect the properties of the rat HD cell system, the model must provide a stable and persistent HD representation robust to noise and must permit the integration of an angular velocity signal.

The model is based upon a continuous attractor/integrator neural network modeling the DTN-LMN interaction. An attractor model of HD cells is a neural network in which units encoding neighboring directions are recursively connected by strong excitatory synapses, whereas units having distant pre-
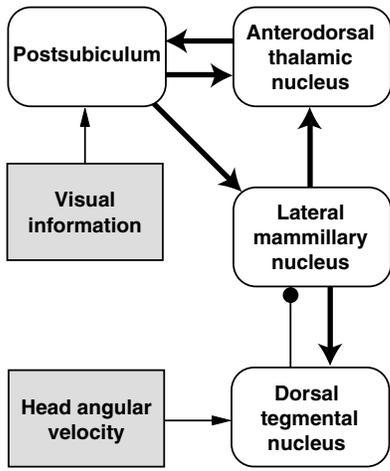
Figure 1: Anatomical connections between the postsubiculum (PSC), the anterodorsal thalamic nucleus (ADN), the lateral mammillary nucleus (LMN) and the dorsal tegmental nucleus (DTN). Arrows and circles indicate excitatory and inhibitory connections, respectively.

Figure 2: A view of the DTN-LMN interaction. An attractor network is formed by the excitatory connections from LMN to DTN (arrows) and the inhibitory connections from DTN to LMN (circles). Also, inhibitory connections within DTN are employed to integrate angular velocity signals.

ferred directions strongly inhibit each other. The interaction between the excitation and the inhibition in the neural network determines the intrinsic dynamics of the attractor. This allows the system to reproduce properties exhibited by rat HD cells. For instance, the system is able to encode a stable HD representation where a subpopulation of HD cells encoding similar directions are active while others remain silent. This HD representation can be updated by extrinsic input signals (e.g. vestibular angular velocity) utilized to shift the ensemble hill of activity of the HD cells over the directional space.

The integration of angular velocity realized by the model is not perfect in a mathematical sense. Consequently, the model needs a calibration method to avoid a cumulative tracking error. We simulate a vision-based calibration by generating an external stimulus applied to the HD cell system. Electrophysiological studies by (Zugaro et al., 2003) have focused on the temporal aspects of the preferred direction update in ADN. The quantitative results show a short update latency of approximately $80 \pm 10\ ms$. Our model uses spiking neurons and allows us to study the temporal aspects of the attractor state transitions. Particularly, the model reproduces the fast update transient exhibited by the rat HD cells observed by (Zugaro et al., 2003).

Several models of HD cells have been previously proposed (Skaggs et al., 1995, Zhang, 1996, Redish et al., 1996, Goodridge and Touretzky, 2000). These models, however, have not been tested by means of robotic implementations. The HD model by (Arleo and Gerstner, 2000) has been validated on a real robot but it uses rate coding computational units which make it impossible to study the dynamics of the system for short time windows. A robotic compass system has been proposed by (Gourichon et al., 2003). However, the authors focus on static visual information only, and do not in-

tegrate angular velocity over time. The model presented here is similar to our previous work (Degris et al., 2004) that puts forth an attractor neural network of spiking neurons to model the DTN-LMN circuit. In contrast to that model, the attractor system presented here does not employ recurrent excitatory projections within the LMN network, consistent with anatomical findings (Allen and Hopkins, 1989). Furthermore, our previous model has been validated by means of numerical simulations only. Here we stress the importance of endowing a mobile robot with a HD system using spiking neurons, and we cope with implementation constraints such as real time performance.
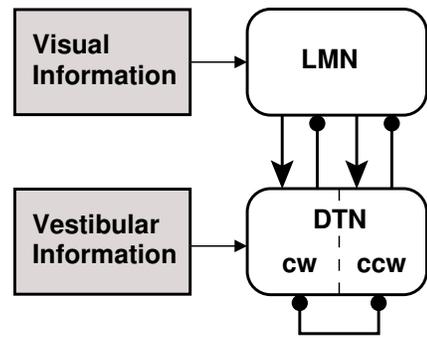
2. Methods

We model HD cells by means of a modular artificial neural network. Fig. 2 shows a view of the model. The architecture consists of an attractor-integrator network composed by a population LMN of $N_E = 1000$ excitatory directional units and two populations DTN_{cw} and DTN_{ccw} of $N_I = 500$ inhibitory directional units each. The HD units within each network have evenly distributed preferred directions.

The dynamics of the HD system is primarily controlled by idiothetic signals (i.e. self-motion inertial inputs) which determine the directional selectivity property of the formal HD cells. Allothetic information (e.g. visual input) can be used to occasionally modify the system's dynamics and calibrate the HD cell activity.

2.1 Robotic Platform

In order to validate the model experimentally, we have implemented it on a mobile Pekee[1] robot (Fig. 3). The behavior of the robot is monitored by an infrared camera above the arena tracking two LEDs positioned on the robot. The relative positions of the two LEDs are sampled at about $60\ Hz$, which

---

[1]The Pekee robot is commercialized by Wany Robotics, http://www.wanyrobotics.com

Figure 3: The mobile Pekee robot with the MT9 device (the black box in front of the robot) for sensing inertial self-motion signals.

Figure 4: The attractor network is based on excitatory connections from LMN to DTN (arrows) and inhibitory connections from DTN to LMN (circles).

allows us to measure the actual orientation $\theta(t)$ of the robot over time.

The robot's sensory system consists of an odometer and a Xsens MT9[2] device for sensing inertial self-motion signals. The MT9 device, composed of gyroscopes, accelerometers and magnetometers, provides a real time absolute orientation resulting of the fusion of the inputs of these sensors.

The low-level controller of the robot runs on the on-board computer, whereas the HD model and the high-level controller run on a remote PC Pentium IV.

2.2 Attractor network

In order to generate and maintain a HD signal $\bar{\theta}$, we consider a continuous attractor network based on the interconnections between LMN and DTN (Blair et al., 1998). Fig. 4 shows the connections between formal neurons in LMN and DTN. Note that, because there is no experimental evidence for lateral connections in LMN (Allen and Hopkins, 1989), there is no recurrent excitation in the LMN of the model (Song and Wang, 2002).

LMN projects excitatory connections to DTN. The weight w_{kn} of these connections is such that a neuron $n \in$ LMN with a preferred direction θ_n projects to a cell $k \in$ DTN with a preferred direction θ_k according to a Gaussian weight distribution

$$w_{kn} = W_e^{max} \cdot \exp\left(-\frac{(\theta_n - \theta_k + \pi + \delta_e)^2}{2\sigma_e^2}\right) \quad (1)$$

where $W_e^{max} = 63.3$ is the maximum weight of excitatory connections and $\sigma_e = 67.2°$ is the width of the Gaussian profile. The values of these parameters have been determined by means of a genetic algorithm (Sec. 2.6). The term δ_e is the angular offset of the intermodule connections with $\delta_e = 50°$ if $k \in$ DTN$_{cw}$ and $\delta_e = -50°$ if $k \in$ DTN$_{ccw}$.

<hr>

[2]The MT9 device is commercialized by Xsens Motion Technologies, http://www.xsens.com

Global inhibition, necessary to implement the center-surround attractor scheme, is provided by the connections from DTN to LMN. The weight w_{nk} of these connections is distributed according to

$$w_{nk} = W_i^{max} \cdot \exp\left(-\frac{(\theta_k - \theta_n)^2}{2\sigma_i^2}\right) \quad (2)$$

where $W_i^{max} = 59.5$ is the maximum weight of inhibitory connections, and $\sigma_i = 147.3°$ is the width of the Gaussian weight distribution (also these two parameters have been set by means of the genetic algorithm described in Sec. 2.6).

Because of the real-time constraint, only the connections with a weight $w > 0.75 * W^{max}$ are actually implemented in the network. This avoids the propagation of spikes along synapses with small weight and drastically reduces the computational complexity of the model. The intrinsic dynamics of the DTN-LMN attractor network settles the system down to stable (self-sustained) attractor states, in which subpopulations of HD cells with similar preferred directions are active while the others remain silent (Zhang, 1996, Blair et al., 1998).

2.3 Integrator

To integrate non-zero angular velocities (i.e. to shift the stable state over the continuous attractor space according to the angular velocity ω), an unbalanced cell activity between DTN$_{cw}$ and DTN$_{ccw}$ is generated. The neuronal responses of the DTN$_{cw}$ and DTN$_{ccw}$ cells are correlated with both the head direction $\theta(t)$ and the angular velocity $\omega(t)$. In particular, the activity of directional cells in DTN$_{cw}$ and DTN$_{ccw}$ is modulated proportionally to $|\omega(t)|$ during clockwise and counterclockwise turning, respectively. Neurons encoding the animal's head angular velocity have been observed in the parietal, somatosensory, and visual cortices (McNaughton et al., 1991, Blair and Sharp, 1995).

Fig. 5 shows the lateral connections between DTN$_{cw}$ and DTN$_{ccw}$. These connections are distributed such that a neuron i with a preferred direction θ_i projects to a cell l with a
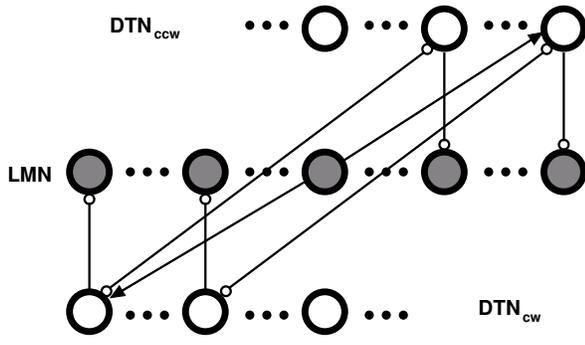
Figure 5: The integrator is based on inhibitory lateral connections (circles) between DTN_{cw} and DTN_{ccw}.

preferred direction θ_l according to

$$w_{li} = W_{li}^{max} \cdot \exp\left(-\frac{(\theta_i - \theta_l + \delta_{li})^2}{2\sigma_{li}^2}\right) \quad (3)$$

where the maximum weight $W_{li}^{max} = 25.6$ and the width $\sigma_{li} = 35.1°$ have been determined by the genetic algorithm (Sec. 2.6). The term δ_{li} is the angular offset of the inter-module connections with $\delta_{li} = -30°$ if $i \in DTN_{cw}$ and $\delta_{li} = 30°$ if $i \in DTN_{ccw}$. Only the connections with a weight $w_{li} > 0.90 * W_{li}^{max}$ are actually implemented in the network.

During clockwise head turns, for instance, DTN_{cw} cells inhibit the left side of the LMN hill of activity encoding the current direction θ (i.e. introduce an asymmetry within the recurrent coupling between LMN and DTN). The lateral shifted connections between DTN_{cw} and DTN_{ccw} reinforce the asymmetry in DTN. During clockwise head turns, DTN_{cw} cells inhibit the left side of the DTN_{ccw} hill. Thus, the inhibition on the right side of the LMN hill is decreased when the inhibition by cells in DTN_{cw} on the left side is increased. This yields a clockwise shift $\Delta\theta$ of the LMN activity profile. The speed of this shift is proportional to $|\omega|$.

2.4 Interpreting the directional output

At each time t, the ensemble activity of a population of neurons provides the estimate $\bar{\theta}(t)$ of the allocentric heading $\theta(t)$ of the robot. In order to compute $\bar{\theta}(t)$, we apply a population vector scheme (Georgopoulos et al., 1986) to decode the ensemble HD cell activity:

$$\theta(t) = \arctan\left(\frac{\sum_n^N sin(\theta_n)\delta(t-t_n)}{\sum_n^N cos(\theta_n)\delta(t-t_n)}\right) \quad (4)$$

where $\delta(t-t_i)$ is a Dirac function equal to 1 if the neuron n fires at time t, 0 otherwise.

2.5 Neuron and synapse model

Both excitatory and inhibitory formal units are leaky integrate-and-fire neurons. Let $V_l = -70\ mV$, $V_t = -50\ mV$, and $V_r = -55\ mV$ denote the resting membrane
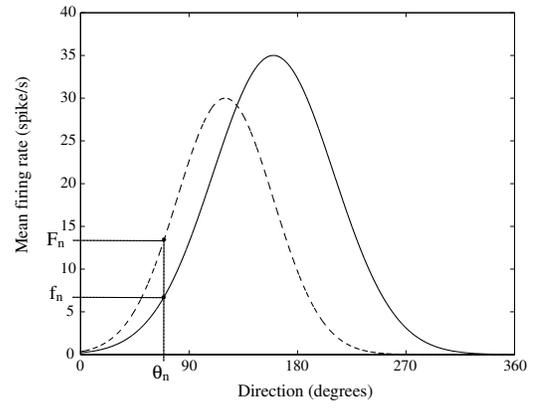
Figure 6: Evaluation of a set of parameters at time t. For each neuron n, the desired Gaussian profile F_n (dashed line) is compared to the generated Gaussian profile f_n (solid line).

potential, the firing threshold, and the reset potential of a formal neuron, respectively. Let $I(t)$ be the total synaptic drive received by a cell from the afferent units. The dynamics of the membrane potential $V(t)$ is given by

$$C \cdot \frac{dV(t)}{dt} = -g \cdot (V(t) - V_l) + I(t) + I_\epsilon(t) \quad (5)$$

where C and g are, respectively, the membrane capacitance and leak conductance ($\tau = C/g$ is the membrane time constant) with $C = 0.5\ \mu F$ for an excitatory cell and $C = 0.2\ \mu F$ for an inhibitory cell; $g_m = 25\ nS$ for an excitatory cell and $g_m = 20\ nS$ for an inhibitory cell. The refractory period is $2\ ms$ and $1\ ms$ for an excitatory neuron and an inhibitory neuron, respectively.

$I_\epsilon(t)$ is the background input activity of a neuron and is defined as

$$I_\epsilon(t) = rnd_{0,1} \cdot K(t) \quad (6)$$

where $rnd_{0,1}$ is a random number uniformly drawn from $[0, 1]$. The factor $K(t)$ is constant for excitatory neurons and equal to 1200. For inhibitory neurons

$$K(t) = K_i + K_\omega \cdot \omega(t) \quad (7)$$

where $K_i = 100$, $K_\omega = 0.44$, and $\omega(t)$ is the angular velocity at time t. The value of K_ω has been determined by the genetic algorithm described in Sec. 2.6.

The synaptic input to a neuron n is taken as

$$I(t) = D \cdot s(t) \quad (8)$$

where $D = 0.01$ is a constant factor and $s(t)$ is a gating variable whose dynamics is given by

$$s(t+\Delta t) = (1-D) \cdot s(t) + \sum_{k=0}^{N} \delta(t-t_k) \cdot w_{nk} + S(n) \quad (9)$$

where $\Delta t = 1\ ms$ is the time step, $\sum_{k=0}^{N} \delta(t-t_k) \cdot w_{nk}$ is a weighted sum over the spikes emitted by the presynaptic neurons k and w_{nk} is the strength of the connection from a presynaptic unit k to the postsynaptic neuron n, with $w_{nk} > 0$ for
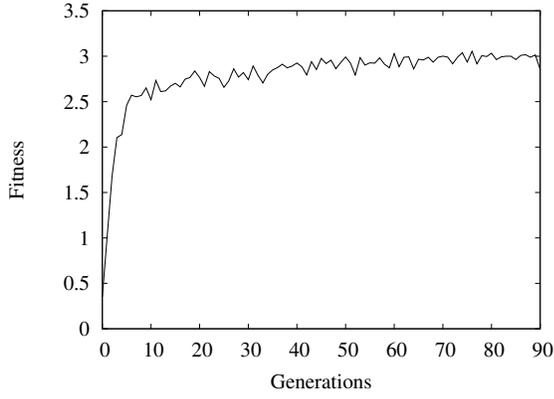
Figure 7: Evolution of the average fitness function over generations.

Figure 8: Emergence of a stable state in LMN in the absence of any polarizing stimulus. The hill of activity is centered at a random direction $\bar{\theta}_e$. Spikes are represented by dots.

excitatory connections and $w_{nk} < 0$ for inhibitory connections. The function $S(n)$ represents a stimulus that can be applied to the excitatory LMN neurons, and defines the number of spikes conveyed by the stimulus to a neuron n at time t. $S(n)$ is distributed over the neurons $n \in$ LMN according to a gaussian profile with amplitude $W_S = 540$ and width $\sigma_S = 90°$.

2.6 Genetic Algorithm

Three sets of Gaussian connections are used in the model: LMN to DTN, DTN to LMN, and the lateral connections between DTN_{cw} and DTN_{ccw}. As seen in Eqs. 1, 2 and 3, two parameters are relevant for determining the weight of a connection: the maximum weight W^{max} and the width of the Gaussian σ. All the six weight parameters as well as the factor K_ω used in Eq. 7 have been determined by using a genetic algorithm in simulation. This learning procedure allowed us to find a set of parameters that provides the model with appropriate stability and integration properties.

The fitness function measures the difference between the desired Gaussian activity profile $F_n(t)$ in LMN and the profile $f_n(t)$ generated by the current set of parameters (Fig. 6). The desired profile function $F_n(t)$ at time t is determined by:

$$F_n(t) = A \cdot \exp^{\frac{-(\theta_n(t) - \theta_\mu(t))^2}{2\sigma^2}} \qquad (10)$$

where $A = 40\ Hz$, $\sigma = 40°$ and $\theta_\mu(t)$ is the current robot direction in the simulation. The fitness function $\phi(t)$ is given by:

$$\phi(t) = \frac{\sum_{n=1}^{N_E} \exp^{\frac{|f_n(t) - F_n(t)|}{k}}}{N} \qquad (11)$$

where $f_n(t)$ is the frequency of the neuron n at time t and $k = 17.4$ a constant.

To improve the selection of appropriate sets of parameters, generations are tested through four different steps M:

1. stability of the model: $\theta_\mu(t) = \theta_{initial}$ is constant and the angular velocity ω is null, $M = 0$,

2. integration of a low angular velocity: $\theta_\mu(t + \Delta t) = \theta_{initial} + \omega \cdot t$ where $\omega \simeq 15°/s$, $M = 1$,

3. integration of a medium angular velocity: $\theta_\mu(t + \Delta t) = \theta_{initial} + \omega \cdot t$ where $\omega \simeq 45°/s$, $M = 2$,

4. integration of a high angular velocity: $\theta_\mu(t + \Delta t) = \theta_{initial} + \omega \cdot t$ where $\omega \simeq 110°/s$, $M = 3$.

Only those neural networks with a fitness $\phi \geq 0.75$ for a given step M are selected and tested in the phase $M + 1$. The final fitness ϕ_P for a given set of parameters P is defined by

$$\phi_P = M + \sum_{t=0}^{T} \frac{\phi(t)}{T} \qquad (12)$$

where T is the duration of the experiment. The evolution of the fitness over generations is shown Fig. 7.

3. Results

First, we study the emergence and stability of a hill of activity to assess the attractor property of the HD model. Second, we study the update of the HD signal based on the integration of an ideal angular velocity input. Third, we apply to the model a real angular velocity signal provided by the MT9 device. Finally, we simulate a visual-based calibration of the system and focus on the latency of the update of the HD cell preferred directions.

3.1 Emergence and stability of an attractor state

The attractor dynamics of the model yields the emergence of a stable state from random noise. Thus, in the absence of external stimuli, the HD population activity profile settles down to a self-sustained state in which only a subpopulation of cells with similar preferred directions discharges tonically. The blob of activity encodes a constant direction $\bar{\theta}_e$ (as shown in Fig. 8). The attractor state is established after a transitory

(a)

(b)
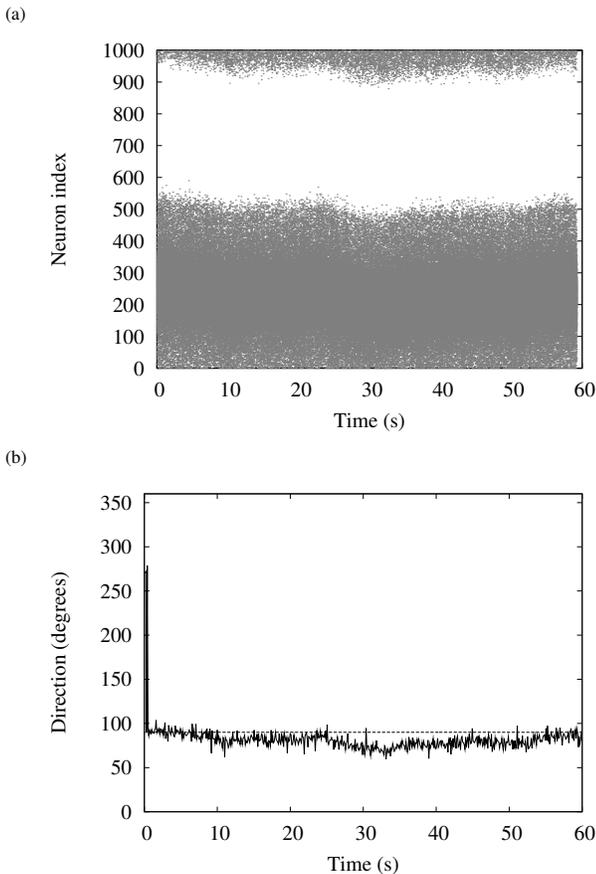
Figure 9: (a) Rastergram of the activity of the HD cells in LMN over 60 s. A polarizing external stimulus (applied at $\theta_S = 90°$ during the first 10 ms) generates a stable attractor state. After stimulus removal ($t > 10$ ms) the self-sustained state persists over time. (b) Stability of the HD representation over time. The dashed line represents the initial direction θ_S set by the stimulus during the first 10 ms. The continuous line is the direction computed by population vector coding (Eq. 4).

period (of approximately 700 ms) characterized by an oscillatory activity pattern. The relative weight between inhibition and excitation determines the equilibrium reached after the transient period.

The model can also be initialized to a specific direction θ_s by applying an external stimulus S to LMN. The rastergram in Fig. 9 (a) shows the spike activity of the N_E cells in LMN when a polarizing input centered at $\theta_S = 90°$ is applied during the first 10 ms. After stimulus removal ($t > 10$ ms), the attractor state persists over the time. This corresponds to the situation in which the head of the animal is immobile (the head angular velocity ω is zero) and oriented in a given direction θ_S. The mean peak spike frequency and the width of the hill of activity, averaged over $T = 60$ s, are about 30 Hz and 200°, respectively.

The center of mass of the ensemble firing pattern, computed according to Eq. 4 and averaging over $T = 60$ s, is
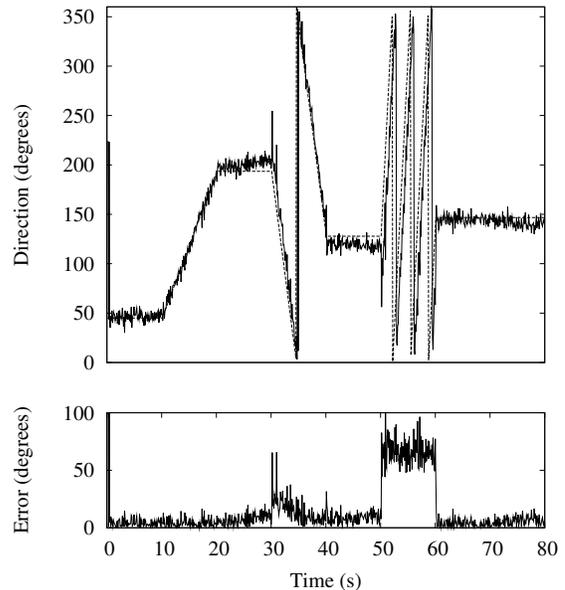
Figure 10: Integration of ideal angular velocities by the model. Top: a velocity $\omega_1 = 15°/s$ is applied for 10 $s < t < 20$ s; a velocity $\omega_2 = 45°/s$ is applied for 30 $s < t < 40$ s; and a velocity $\omega_3 = 110°/s$ is applied for 50 $s < t < 60$ s. The dashed line represents the ideal integration of these angular velocities. The continuous line represents the direction signal of the HD cells of the model. Bottom: the integration error of the HD system over time.

about $\bar{\theta} = 86°$. Fig. 9 (b) shows the stability of the directional representation over 60 s. The mean error $e = \sum_t \left| \bar{\theta}(t) - \theta_S \right| / T$ is about 9°.

3.2 Integration

When the head of the rat rotates (i.e. $\omega \neq 0$), the HD cell system integrates the angular velocity in order to update the HD representation over time.

We first investigate the integration done by the model in the case of three ideal angular velocity signals, $\omega_1 = 15°/s$, $\omega_2 = 45°/s$ and $\omega_3 = 110°/s$. Each angular velocity input is applied during a 10 s period. Fig. 10 shows the response of the HD cell system to these three velocity profiles as well as the integration error over time. The average error of the estimation of the direction by the model is about 12°. Qualitatively, the diagram shows that the larger the angular velocity, the larger the error.

The above simulation does not reflect the noise present in real experimental conditions. For instance, when sending a motor command to the robot, the motion generated by the actuators is noisy. Fig. 11 compares an ideal angular velocity profile (motor command) to the real angular velocity of the robot. The robot is asked to turn on the spot at different random speeds for different random time periods. The angular velocity of the robot is computed from the absolute direction given by the video tracking system. The comparison shows
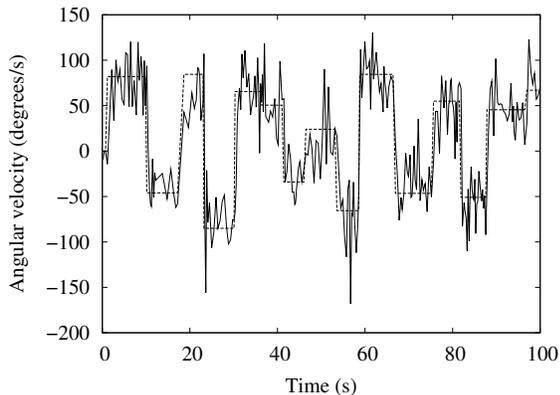
Figure 11: Example of noisy angular velocity profile. The dashed line represents the command sent to the robot. The continuous line indicates the angular velocity computed by the tracking system.

that, given a constant angular velocity command, the real angular velocity of the robot is unstable.

Since the navigating robot has to be able to estimate its current heading autonomously, it must integrate the angular velocity signals coming from of one of the on-board sensory systems. The robot is equipped with odometers measuring locomotor signals and accelerometers (the MT9 device) providing inertial signals.

Fig. 12 compares the real direction of the robot (provided by the video tracking system) and the directions computed by the MT9 device and by the odometers. The experimental protocol is the same as the one used previously. Let $e = \sum_t |\theta'(t) - \theta(t)|/T$ denote the mean error, averaged over $T = 100\ s$, between the estimation $\theta'(t)$ and the actual direction $\theta(t)$ of the robot. We average e over 26 trials and find an error of $e_{MT9} = 64°$ for the directional signal from the MT9 device and an error of $e_{odo} = 71°$ for the odometers.

Note that, given the experimental protocol (a robot rotating on the spot), non-systematic errors, like wheel slippage or irregularities on rough surface, are unlikely to occur. Despite the small difference between e_{MT9} and e_{odo}, the angular velocity input provided by the MT9 device is more reliable than the signal from the odometers. For instance, if the robot was pulled up and displaced passively by the experimenter, the odometry would be seriously impaired whereas the MT9 device would be able to sense the movement. Therefore, we decided to use the MT9 device signal as input for our HD model.

At time $t = 0$, the HD system is initialized with respect to an absolute direction θ_{MT9}. As the robot starts rotating, the signals from the MT9 device are integrated by the model which starts shifting its internal representation to track the angular displacements of the robot. Fig. 13 shows an example of the update of the HD signal $\bar{\theta}(t)$ encoding the current robot heading $\theta(t)$ as well as the tracking error over time. The mean error of the model, over 26 trials of $T = 100\ s$ each, is $33°$ relative to the input of the MT9 device and about $73°$ relative

(a)

(b)
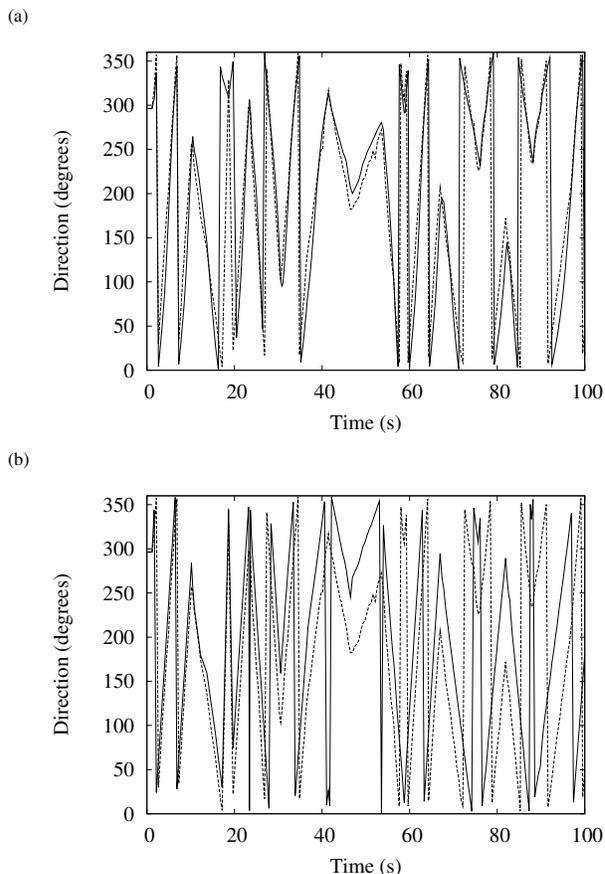
Figure 12: Tracking of the robot actual direction (represented by the dashed line) by the MT9 device (a) and by the integration of the input from the odometers (b).

to the output of the video tracking system.

As shown in Fig. 13, the integration realized by the model is not perfect in a mathematical sense. Thus, the system needs to be calibrated to avoid cumulative errors over time. In this paper, we do not describe any calibration mechanism (Arleo and Gerstner, 2000). Rather, we focus on the temporal aspects of the update of the preferred directions of HD cells by a reorienting visual stimulus.

3.3 Short update latencies following reorienting stimuli

Electrophysiological findings suggest that HD cells are controlled by salient visual cues (Taube, 1998). Recently, (Zugaro et al., 2003) have measured the time necessary to update the preferred directions of rat HD cells by a reorienting visual landmark. The experimental setup consisted of a black cylinder with a white card attached to the inner wall used as a visual cue. The preferred directions of the HD cells were first measured in light conditions. Then, in the dark, the cue card was rotated by $90°$. When, the light was turned back on the HD cells updated their preferred directions to reflect the
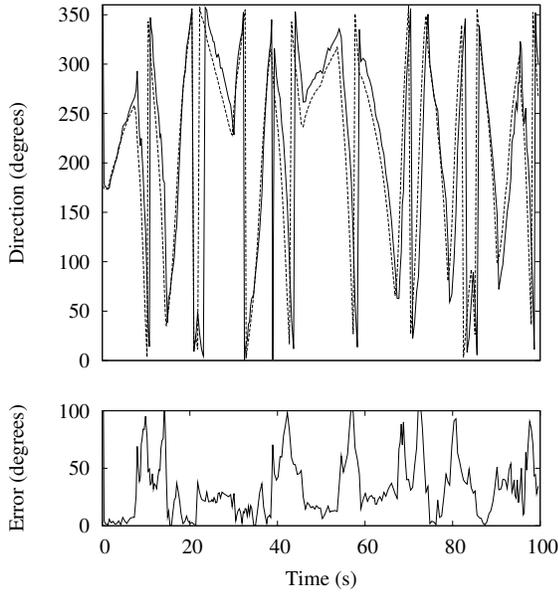
Figure 13: Update of the HD directional coding by the model (continuous line) by integrating the signal provided by the MT9 device (dashed line). The error of integration of the model compared to the direction given by MT9 is shown in the diagram below.

Figure 14: Raster plot showing the response of the HD system to a $180°$ reorienting visual stimulus applied at time $t_{S'} = 5\ s$. A new blob of activity is established at $\theta_{S'} = 270°$ whereas the previous hill of activity is extinguished.

new visual configuration. A mean latency of $80 \pm 10\ ms$ was observed for the establishment of a new blob following the reorientation event. On the other hand, $140 \pm 10\ ms$ were necessary for the extinction of the hill of activity existing prior the reorientation event.

To reproduce these results, the model is first initialized with an external stimulus S centered at a specific direction $\theta_S = 90°$. Second, at time $t_{S'} = 5\ s$, a reorienting stimulus S' is applied at $\theta_{S'} = 270°$ (simulating the transition from dark to light conditions). Fig. 14 shows the response of the system to the reorienting visual stimulus which triggers a $180°$ update of all preferred directions. The HD system is reoriented according to the directional reference frame anchored to S'. As a consequence, the attractor network settles to a new stable state abruptly.

The resulting update latency for the establishment of the new blob of activity is about $30\ ms$, whereas the transient delay for the extinction of the previous attractor state is about $110\ ms$. The attractor dynamics is such that inhibition occurs after the increase in the overall activity of the network. This causes a longer update time for the extinction of the previous hill of activity. These results are consistent with those reported by (Zugaro et al., 2003). Note that in the model the transmission delay necessary for the visual signals to reach HD cells is not taken into account. There are no experimental data reporting this transmission delay. However, (Galambos et al., 2000) show that a visual stimulus takes already about $30\ ms$ to go from the retina to the primary visual cortex.

4. Discussion

The main goal of this work was to endow a robot with an allocentric direction representation. We adopted a neuro-mimetic approach inspired by the properties of head direction (HD) cells, neurons observed in the rat's limbic system.

In order to obtain a stable and persistent HD signal, the model relies on an attractor neural network modeling the neural circuit formed by the lateral mammillary nucleus (LMN) and the dorsal tegmental nucleus (DTN). These two anatomical structures are relevant for generating and maintaining the internal direction representation of rat HD cells. The model reproduces the anatomical interconnectivity between LMN and DTN. The attractor network has no lateral excitatory connections to reflect the absence of experimental evidence for recurrent excitation in the DTN-LMN circuit. Similar to the rat HD cell system, the model can integrate angular velocity signals to update the direction representation over time. Lateral inhibitory connections in the formal DTN are used for this purpose.

In contrast to earlier HD models, we employ spiking neurons to focus on the temporal aspects of the dynamics of the attractor network. For instance, electrophysiological data suggest a very rapid reorientation of the HD representation following changes in the visual scene. The model is able to reproduce these short update latencies.

We stress the importance of validating the model in real experimental conditions in order to make it useful for autonomous navigating systems. We assess the ability of the model to integrate an angular velocity signal $\omega(t)$ in realtime. We employ an inertial sensor to estimate the angular displacements of the robot. The integration of $\omega(t)$ is affected by a drift of the internal direction representation over time. Therefore, a calibration mechanism, based for instance on vision, will be further developed. Experimental findings show that visual information is conveyed to the HD system via the

postsubiculum (PSC). The model may be extended by adding a PSC module performing the vision-based calibration.

The HD model presented here provides a subcomponent for a larger autonomous navigating system. This work is part of Psikharpax, a project that aims at developing a bio-mimetic navigation and action selection model embedded on a real robot.

Acknowledgments

References

Allen, G. V. and Hopkins, D. A. (1989). Mamillary body in the rat: topography and synaptology of projections from the subicular complex, prefrontal cortex, and midbrain tegmentum. *Journal of Comparative Neurology*, 286:311–336.

Arleo, A. and Gerstner, W. (2000). Modeling rodent head-direction cells and place cells for spatial learning in bio-mimetic robotics. In Meyer, J.-A., Berthoz, A., Floreano, D., Roitblat, H., and Wilson, S. W., (Eds.), *From Animals to Animats VI*, pages 236–245, Cambridge MA. MIT Press.

Bassett, J. P. and Taube, J. S. (2001). Neural correlates for angular head velocity in the rat dorsal tegmental nucleus. *The Journal of Neuroscience*, 21(15):5740–5751.

Blair, H. T., Cho, J., and Sharp, P. E. (1998). Role of the lateral mammillary nucleus in the rat head direction circuit: A combined single unit recording and lesion study. *Neuron*, 21:1387–1397.

Blair, H. T. and Sharp, P. E. (1995). Anticipatory head direction signals in anterior thalamus: Evidence for a thalamocortical circuit that integrates angular head motion to compute head direction. *The Journal of Neuroscience*, 15(9):6260–6270.

Degris, T., Brunel, N., Sigaud, O., and Arleo, A. (2004). Rapid response of head direction cells to reorienting visual cues: A computational model. *Neurocomputing (in press)*.

Galambos, R., Szabo-Salfay, O., s, P. B., Palhalmi, J., Szilagyi, N., and Juhasz, G. (2000). Temporal distribution of the ganglion cell volleys in the normal rat optic nerve. *Proceedings of the National Academy of Sciences USA*, 97(24):13454–13459.

Georgopoulos, A. P., Schwartz, A., and Kettner, R. E. (1986). Neuronal population coding of movement direction. *Science*, 233:1416–1419.

Goodridge, J. P. and Touretzky, D. S. (2000). Modeling attractor deformation in the rodent head-direction system. *Journal of Neurophysiology*, 83(6):3402–3410.

Gourichon, S., Meyer, J.-A., Ieng, S., Smadja, L., and Benosman, R. (2003). Estimating ego-motion using a panoramic sensor: Comparison between a bio-inspired and a camera-calibrated method. In Holstein, H. and Labrosse, F., (Eds.), *AISB03 Symposium on Biologically Inspired Vision, Theory and Application*, pages 91–101.

Knierim, J. J., Kudrimoti, H. S., and McNaughton, B. L. (1995). Place cells, head direction cells, and the learning of landmark stability. *The Journal of Neuroscience*, 15:1648–1659.

McNaughton, B. L., Chen, L. L., and Markus, E. J. (1991). Dead reckoning, landmark learning, and the sense of direction: A neurophysiological and computational hypothesis. *Journal of Cognitive Neuroscience*, 3:190.

Mittelstaedt, M. L. and Mittelstaedt, H. (1980). Homing by path integration in a mammal. *Naturwissenschaften*, 67:566–567.

Redish, A. D., Elga, A. N., and Touretzky, D. S. (1996). A coupled attractor model of the rodent head direction system. *Network*, 7(4):671–685.

Skaggs, W. E., Knierim, J. J., Kudrimoti, H. S., and McNaughton, B. L. (1995). A model of the neural basis of the rat's sense of direction. In Tesauro, G., Touretzky, D. S., and Leen, T. K., (Eds.), *Advances in Neural Information Processing Systems 7*, pages 173–180, Cambridge, MA. MIT Press.

Song, P. and Wang, X.-J. (2002). An attractor network model without recurrent synaptic excitation for head direction neurons in rodents. *Society for Neuroscience Abstracts*, page 584.8.

Taube, J. S. (1998). Head direction cells and the neurophysiological basis for a sense of direction. *Progress in Neurobiology*, 55:225–256.

Zhang, K. (1996). Representation of spatial orientation by the intrinsic dynamics of the head-direction cell ensemble: A theory. *The Journal of Neuroscience*, 16(6):2112–2126.

Zugaro, M. B., Arleo, A., Berthoz, A., and Wiener, S. I. (2003). Rapid spatial reorientation and head direction cells. *The Journal of Neuroscience*, 23(8):3478–3482.

Zugaro, M. B., Berthoz, A., and Wiener, S. I. (2001). Background, but not foreground, spatial cues are taken as references for head direction responses by rat anterodorsal thalamus neurons. *The Journal of Neuroscience*, 21(RC154):1–5.